Evaluation of the Effect of CO_2 Cover Gas on the Rate of Oxidation of an AlMgSi Alloy

Cathrine Kyung Won Solem, Kai Erik Ekstrøm, Gabriella Tranell, and Ragnhild E. Aune

Abstract

Small additions of beryllium (Be) to aluminum magnesium (AlMg) alloys have proven to decrease their oxidation rate during industrial liquid metal handling. As Be can cause respiratory health issues, it is desirable to evaluate alternative methods to inhibit the oxidation rate. Earlier work has revealed that small amounts of carbon dioxide (CO_2) to the surrounding atmosphere has a positive effect. In the present study the oxidation behavior of an aluminum magnesium silicon (AlMgSi) alloy has been investigated using a Differential Scanning Calorimetric (DSC) unit equipped with a Thermogravimetric Analyzer (TGA). Changes in both the heat flux and the mass have been monitored during exposer to 20% argon (Ar) and 80% *synthetic air*, 99.999% pure *Ar*, and a gaseous mixture of 20% Ar, 76% synthetic air and 4% CO_2 at 750 °C for 7 h. The results revealed a one-step mass gain when heated in *synthetic air*, giving a total mass gain of 12.33% and an oxide layer thickness of >15 µm. Pure *Ar* had a positive effect on the oxidation rate lowering the mass gain to 2.80% and a thickness of ~10 µm. A mass gain of only 0.46% and a continuous dense oxide layer of 200–400 nm, with an additional granular discontinuous oxide layer of ~2 µm underneath, was obtained during heating in 4% CO_2. This confirms that even in the case of the AlMgSi alloy, small amounts of CO_2 have a significant inhibiting effect on the oxidation rate.

Keywords

AlMgSi alloy • Oxidation • Breakaway oxidation • Ar • Synthetic air • CO_2

Introduction

Aluminum (Al) alloys are used in numerous applications such as transportation, packaging and building constructions [1]. During liquid processing, the Al alloys oxidize when exposed to oxidizing atmospheres, e.g. air [1–4], resulting in significant metal losses ranging from 1 to 10% of the melt [5].

Aluminum magnesium (AlMg) alloys is a common group of materials that are typically used in automotive applications, in maritime environments, and in beverage cans. Their frequent use is mostly due to their corrosion resistance.

Oxidation of AlMg Systems

Over the years, the oxidation of AlMg alloys has been extensively studied by several researchers, including the influence of atmosphere on the rate and product of oxidation [1, 3, 6–9]. The early work of Cochran and Sleppy [10] established that aluminum alloys containing Mg have a significantly higher mass gain than high-purity aluminum when exposed to air [10]. Further investigations monitoring the mass as a function of time and temperature while exposing it to different cover gases, e.g. air containing water vapor [10] and dried air [11], revealed that the mass gain of AlMg alloys is identified by a two-step mass gain process. Firstly, a linear mass gain is obtained due to the formation of a granular magnesium oxide (MgO) layer, and secondly, a rapid breakaway oxidation mass gain due to the formation of magnesium aluminate spinel ($MgAl_2O_4$) [2, 7, 11], characterized by nodules covering the surface, as well as "cauliflower" shaped topography [12, 13]. In Eqs. (1) and (2) the reactions occurring with respect to one mole O_2 (g), with a decrease in Gibbs Energy (ΔG^0), are presented [14].

$$2/3\,MgO + 4/3\,Al + O_2(g) = 2/3\,MgAl_2O_4 \qquad \Delta G^0_{750\,^\circ C} = -925.66\ kJ \tag{1}$$

C. K. W. Solem (✉) · K. E. Ekstrøm · G. Tranell · R. E. Aune
Department of Materials Science and Engineering, Norwegian University of Science and Technology (NTNU), Trondheim, Norway
e-mail: cathrine.k.w.solem@ntnu.no

A. Tomsett (ed.), *Light Metals 2020*, The Minerals, Metals & Materials Series,
https://doi.org/10.1007/978-3-030-36408-3_154

$$2\,\mathrm{Mg} + \mathrm{O_2(g)} = 2\,\mathrm{MgO}$$
$$\Delta G^0_{750\,^\circ\mathrm{C}} = -981.64\ \mathrm{kJ} \quad (2)$$

Oxidation of AlMgSi Systems

Over the years it has been reported in literature that additions of Mn, Fe, Cu and Si to Al do not have a significant effect on the rate of oxidation in regard to binary Al systems [12]. However, for higher order systems, it is not well understood how these elements effect the oxidation rate, or what oxides that are formed in which order. Two different oxide formation processes have been suggested, i.e. the formation of (i) an Al–Mg–O oxide rich in MgO, and (ii) aluminum oxide (Al_2O_3) together with other oxides, but in both cases Si is only present as a trace element and not as a pure component in the oxide [12].

When looking at the formation of Mg_2Si at 750 °C, the ΔG^0 is significantly higher than for SiO_2, Mg_2SiO_4 and Al_2O_3. From a thermodynamic point of view, this indicates that Mg_2Si will not be favored at this temperature, see Eqs. (3)–(6) [14].

$$2\,\mathrm{Mg} + \mathrm{Si} = \mathrm{Mg_2Si}$$
$$\Delta G^0_{750\,^\circ\mathrm{C}} = -66.93\,\mathrm{kJ} \quad (3)$$

$$\mathrm{Si} + \mathrm{O_2(g)} = \mathrm{SiO_2}$$
$$\Delta G^0_{750\,^\circ\mathrm{C}} = -726.17\ \mathrm{kJ} \quad (4)$$

$$2\,\mathrm{MgO} + \mathrm{Si} + \mathrm{O_2(g)} = \mathrm{Mg_2SiO_4}$$
$$\Delta G^0_{750\,^\circ\mathrm{C}} = -785.23\,\mathrm{kJ} \quad (5)$$

$$4/3\,\mathrm{Al} + \mathrm{O_2(g)} = 2/3\,\mathrm{Al_2O_3}$$
$$\Delta G^0_{750\,^\circ\mathrm{C}} = -902.53\,\mathrm{kJ} \quad (6)$$

In Fig. 1a and b the Al–Mg–O_2–Si phase diagram is presented as a function of the partial pressure of O_2 with respect to the activity of Mg and Al in the melt, respectively [15]. As can be seen from the phase diagrams, there are several different oxides that may be formed at the temperature of interest, i.e. (i) depending on the activity of Mg in the Al melt, Al_2O_3 and $MgAl_2O_4$ (SPIN) are stable together with pure Si (s), (ii) at higher partial pressures, Mg_2SiO_4 is stable together with $MgAl_2O_4$, (iii) when the activity of Al in the melt is low, $MgAl_2O_4$ and Si (s) are stable, and (iv) there may be an equilibrium between Mg_2Si and MgO, with no Al present in neither of the phases.

Inhibition of the Oxide Layer

Small additions (2–200 ppm) of Be to AlMg alloys have proven to have an inhibiting effect on the formation of the oxide layer, and thereby also on the overall rate of oxidation during processing [1, 3, 13]. Smith et al. [13] reported recently that with an addition of 100 ppm Be to an AlMg5 alloy heated in air at 700 °C for 6 h, a granular MgO layer was formed on the surface of the material with an additional thin beryllium oxide (BeO) layer underneath. The BeO layer inhibited the transport of Mg from the bulk through the oxide, hence, limiting the oxidation and the formation of $MgAl_2O_4$, i.e. the second mass gain step was avoided. Be is, however, well-known for being hazardous, causing respiratory health

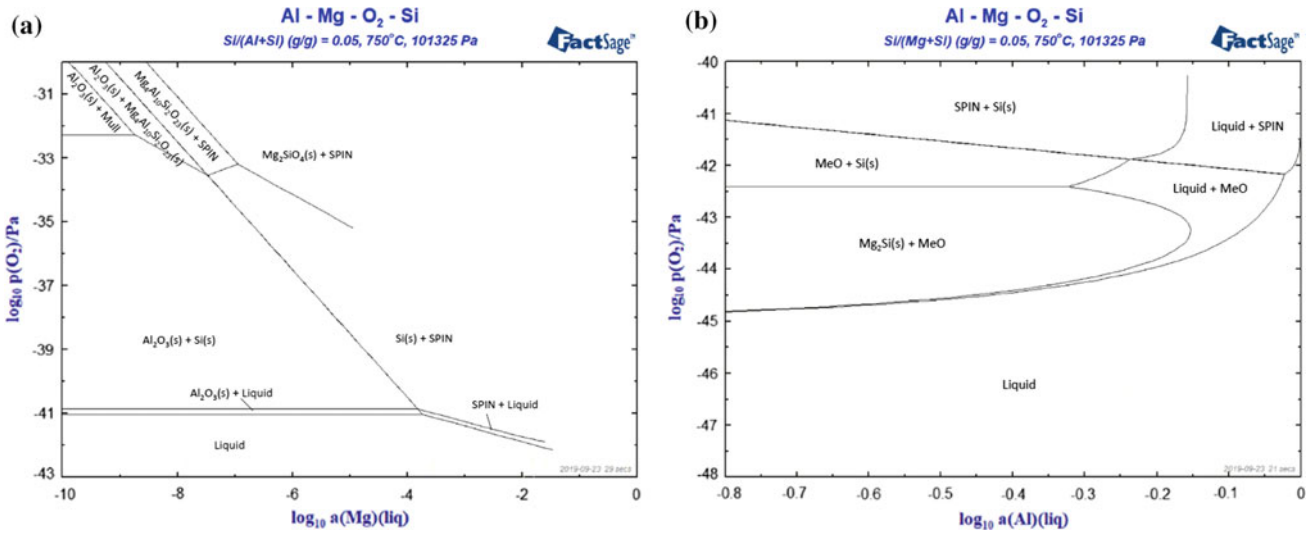

Fig. 1 Al–Mg–O_2–Si phase diagram as a function of the activity of the partial pressure of O_2 at 750 °C with respect to **a** the activity of Mg and **b** the activity of Al in the melt, where $MgAl_2O_4$, Al_2SiO_5 and MgO are referred to as Mull, SPIN and MeO, respectively [15]

issues, thus, it is desirable to evaluate alternative methods of inhibiting oxidation of AlMg-based alloys.

CO_2 has been investigated as a protective cover gas for AlMg alloys, both as pure gas and in gaseous mixtures with air, water vapor and Ar. Additions of small amounts of CO_2 have proven to have an inhibiting effect on the onset of breakaway oxidation [2, 4], limiting the evaporation of Mg from the bulk metal through the formed MgO oxide layer. In the case of AlMg5, concentrations as low as 5% CO_2 in the cover gas gave a pronounced protective effect (comparable to 20% CO_2 in both Ar and air), which resulted in a mass gain <0.5% when heated at 750 °C for 7 h. The thin oxide layer formed on the alloy contained carbon, where the ratio between O and C was found to decrease towards the oxide-alloy interface as a result of Mg reducing the CO_2 gas [2].

While the oxidation behavior of the AlMg system is partly understood, there is still a lack of knowledge in regards to the oxidation of higher order AlMg-based systems. Therefore, in the present study, the oxidation of an AlMgSi alloy will be investigated through Differential Scanning Calorimetry (DSC) equipped with a Thermogravimetric Analyzes (TGA). Special attention will be given to the effect that silicon (Si) has on the morphology and composition of the oxide layer, as well as the overall rate of oxidation during exposure to different cover gases, i.e. (i) 20% Ar and 80% synthetic air, (ii) pure Ar, and (iii) a gaseous mixture of 20% Ar, 76% synthetic air and 4% CO_2.

Experimental

Sample Preparation

The AlMgSi alloy investigated was tailored from 99.999% pure Al (Alfa Aesar), 99.98% pure Mg (Sigma Aldrich) and 99.9999% pure Si (Wacker). The elements were placed layer by layer in an Al_2O_3 crucible with an inner diameter of 45 mm, i.e. the bottom was covered by a layer of Al, followed by a layer of Mg and Si and finished off with another layer of Al. The crucible was later placed in a vacuum induction furnace in an inert atmosphere of 99.999% pure Ar, heated to 850 °C and held for 30 min to ensure homogeneous distribution of the elements in the alloy (theoretical melting temperature is 556 °C [15]). After the isothermal segment, the furnace was turned off and the alloy was naturally cooled to ambient temperature inside the furnace. The alloy was separated from the crucible and milled to remove any residues securing a clean metal surface. In Table 1 the trace elements present in the master alloy, as well as the quantitative data from the chemical analysis performed with a Nu Instrument Astrum Glow Discharge Mass Spectrometry (GDMS), is presented.

The alloy was then cut into 1.5 mm thick plates, which later were cut into small discs having a diameter of ~3–4 mm, before being polished to 5 µm grid. After polishing, the samples were stored in ethanol until the experiments were carried out in a Simultaneous Thermal Analyzer (STA).

Differential Scanning Calorimetry with Thermogravimetric Analysis (DSC-TG)

A NETZSCH Simultaneously Thermogravimetric Analyzer (STA) model 449 F Jupiter apparatus having a Differential Scanning Calorimetric (DSC) set up was used to monitor the heat flux and mass change of the discs as a function of time and temperature. Three parallel experiments for each cover gas, i.e. (i) 99.999% pure Ar (from here on referred to as Ar), (ii) 20% pure Ar and 80% synthetic air (from here on referred to as synthetic air), and (iii) a gaseous mixture of 20% pure Ar, 76% synthetic air and 4% CO_2 (from here on referred to as 4% CO_2) were carried out to confirm reproducibility of the results. The DSC-TG trials were conducted with a heating and cooling rate of 10 °C/min and a dwell time of 7 h at 750 °C using Al_2O_3 crucibles with an inner diameter of 6 mm. The typical operating temperature used in cast houses during production of Al is ~750 °C and therefore the temperature chosen for the isothermal sections during the DSC-TG trials.

Microscopy

A Zeiss Ultra 55 Limited Edition Secondary Electron Microscope (SEM) was used to investigate the surfaces of the discs after the DSC-TG analyzes, and a FEI Helios NanoLab Dual Focused Ion Beam (FIB) was used to visualize the cross sections, i.e. the oxide layers, for further evaluation. The cross sections were also investigated using Energy Dispersive Spectroscopy (EDS) for elemental mapping.

Table 1 Chemical analyses given in weight percentage (wt%) of the AlMgSi alloy based on Glow Discharge Mass Spectrometry (GDMS) analysis

	Al	Mg	Si	Fe	Cu	Ca	Mn
AlMgSi (wt%)	Balance	6.7670	6.6933	0.0087	0.0087	0.0003	0.0002
Std. dev. (%)	–	0.1786	0.1650	0.0001	0.0002	0.0000	0.0000

Results and Discussion

The mass gain (TGA) of the AlMgSi discs heated at 750 °C for 7 h in the three different cover gases investigated in the present study, i.e. synthetic air, Ar, and 4% CO_2, is presented in Fig. 2a. As can be seen from the figure, a significant increase in the mass was obtained for the discs heated in synthetic air (dotted gray graph), resulting in an average of 12.33% having a standard deviation of 0.22%. An inhibitition of the rate of oxidation was obtained when heating the discs in Ar resulting in a mass gain of 2.80% with a standard deviation of 0.08%, and even greater for 4% CO_2 resulting in an increase of only 0.46% with a standard deviation of 0.11%.

In Fig. 2b the mass gain and the heat flux for the AlMgSi discs heated in synthetic air are presented. As can be seen from the figure, a significant mass gain is observed after ~2 h, confirmed by deep negative heat fluxes indicating that exothermic reactions had taken place, e.g. through Eqs. (1) and (2). It can be noted that even though the mass gain is only in one step and not two well-defined separated peaks as reported in the literature, the heat flux consists of several peaks indicating that more than one reaction had occurred. The microscopic analysis of the surface morphology reveals the formation of granular MgO particles on the surface of the heated discs, see Fig. 3a, similar to the cauliflower shaped nodulus recognized from literature. The cross section of the oxide layer presented in Fig. 4a reveals the existence of an oxide layer (light gray areas), where the density of the oxide layer decreases with increasing depth in the sample. The total thickness of the layer is, however, believed to be thicker than what is visible in the figure, i.e. >15 µm. The EDS results reveals that Al, Mg and O is present in the oxide layer closest to the surface of the heated discs, a Si rich area deeper in the oxide layer, and high concentrations of Al in the lowest area of the cross section. This indicates the formation of MgO and $MgAl_2O_4$, and a phase containing Si, O and Mg closest to the bulk metal, e.g. Mg_2SiO_4. Although the oxide layer was established to be thicker when heating the discs in synthetic air than in Ar, the discs had less charging in SEM, implying a higher conductivity in the case of these dicsc. This may be explained by the smooth areas in between the granular oxide layer, see Fig. 3a, resulting in a thinner oxide layer increasing the

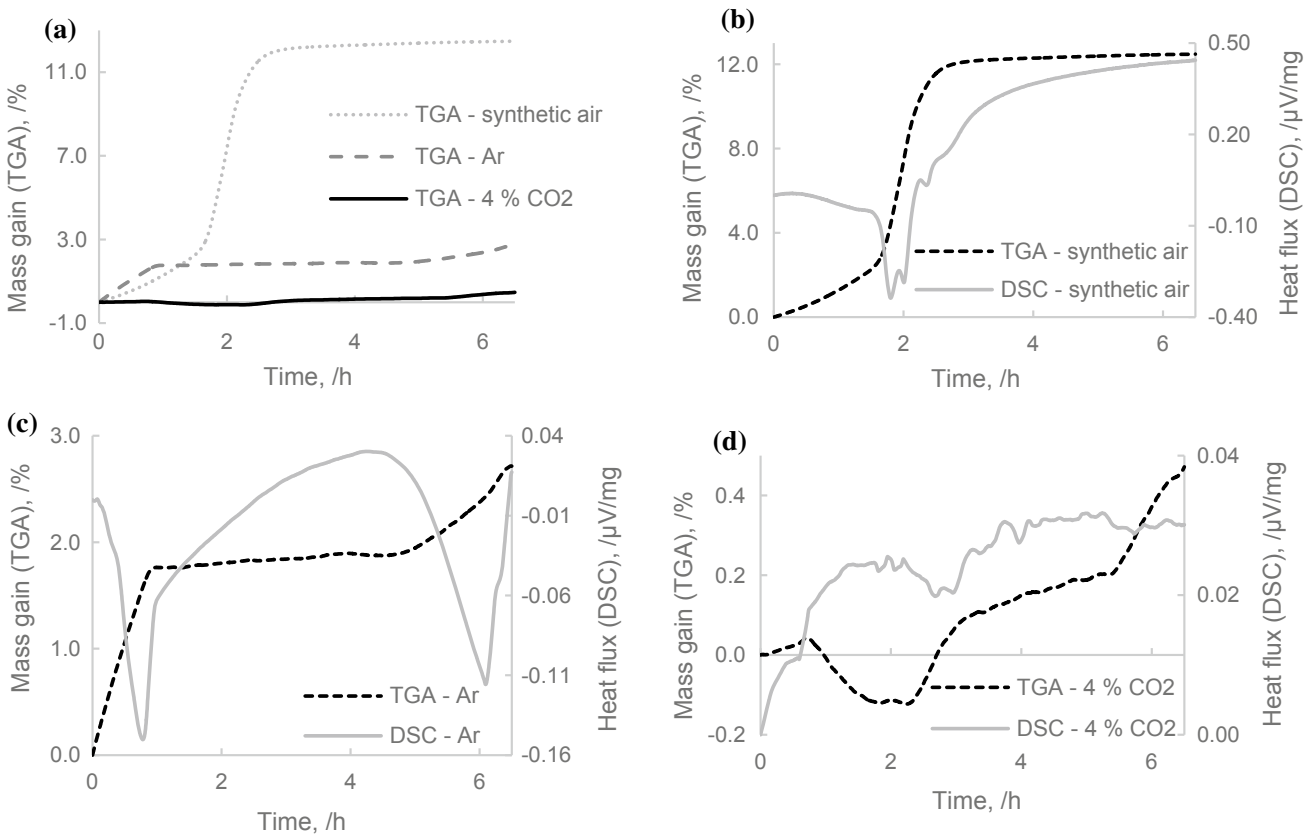

Fig. 2 DSC-TG results for AlMgSi discs heated at 750 °C for 7 h. **a** The mass gain (TGA) of the discs when heated in synthetic air (dotted gray graph), Ar (dashed gray graph), and 4% CO_2 (straight black graph). **b–c** The mass gain (TGA, dashed black graphs) and the heat flux (DSC, straight gray graphs) when heated in synthetic air, Ar and 4% CO_2. All graphs have been plotted from the time the temperature had stabilized at 750 °C, and negative heat flux peaks represent exothermic reactions

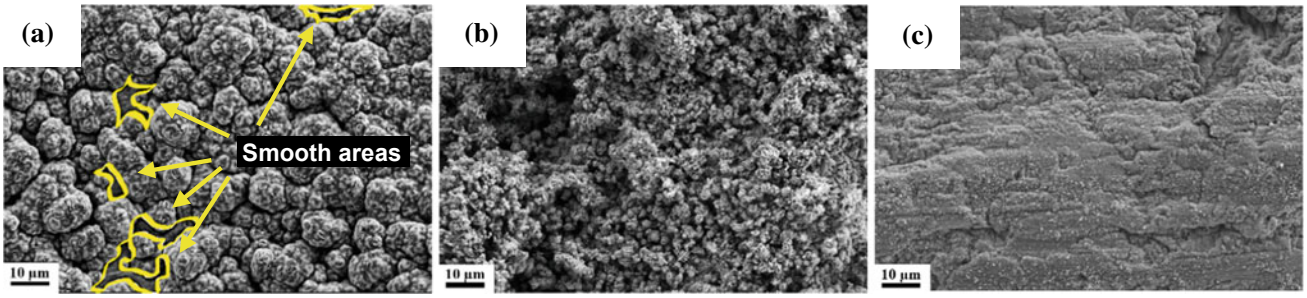

Fig. 3 Secondary Electron Microscopy (SEM) images with a magnification of 1000X of AlMgSi discs heated at 750 °C for 7 h in **a** synthetic air where the surface is covered by granular oxide with some smooth areas in between (see yellow areas). **b** Ar where the surface is covered by granular oxide, and **c** 4% CO_2 where the surface is covered by fine particles and a rougher horizontal structure/texture with some smooth areas in between

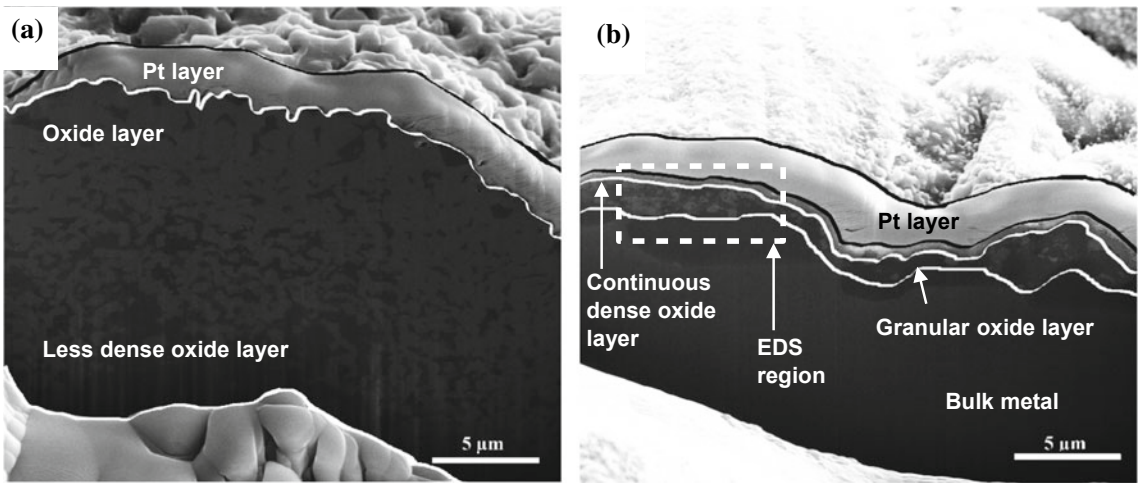

Fig. 4 The cross sections of the AlMgSi discs heated at 750 °C for 7 h with a magnification of 5000X based on SEM images obtained using a Focused Ion Beam (FIB) instrument, where **a** shows a disc heated in synthetic air where the oxide (light gray) is partly integrated in an Al matrix (dark gray), and **b** a disc heated in 4% CO_2 revealing a thin continuous dense oxide layer with an additional granular oxide layer underneath. The dashed rectangular shows the region where the Energy Dispersive Spectrometry (EDS) analysis was performed

conductivity of the electron beam. In addition, these areas may be the result of breakaway oxidation, i.e. the formation of $MgAl_2O_4$, which partly occurs simultaneously with the formation of MgO.

In Fig. 2c the mass gain and the heat flux for the AlMgSi discs heated in Ar are presented. As can be seen from the figure, a two-step mass gain is obtained for the heated discs, where the first linear mass gain stabilizes after ~50 min, before increasing again after ~5 h. This is also identified by the heat flux, revealing two exothermic (negative) peaks, which indicates that there are stable oxides spontaneously generated on the surface of the heated discs, e.g. through Eqs. (1) and (2). When looking at the surface morphology in Fig. 3b, a homogeneous layer consisting of small nods similar to those obtained for the discs heated in synthetic air is obtained. The EDS analysis of the cross section reveals the formation of an oxide layer with a total thickness of ~10 µm. The presence of Mg and O in the oxide layer is confirmed, indicating that the formation of MgO had taken place, which justifies the rapid linear mass gain seen from the dashed black graph in Fig. 2c. For the second mass gain step seen in the same figure, hardly any Al was detected, implying the absence of $MgAl_2O_4$, which is identified to be the product of the second mass gain for AlMg alloys when exposed to oxidizing atmospheres. However, the initial stage of the second mass gain after ~5 h, indicates that the formation of $MgAl_2O_4$ may not be finalised as the mass was still increasing after 7 h. No indication of Mg_2SiO_4 was detected in this sample.

When adding 4% CO_2 in the cover gas, a significantly drop in the mass gain of the heated discs is observed, see Fig. 2d. A total mass change of only 0.46% is measured for the isothermal segment, and only one well-defined negative heat flux peak is identified after ~3 h. However, the peak is

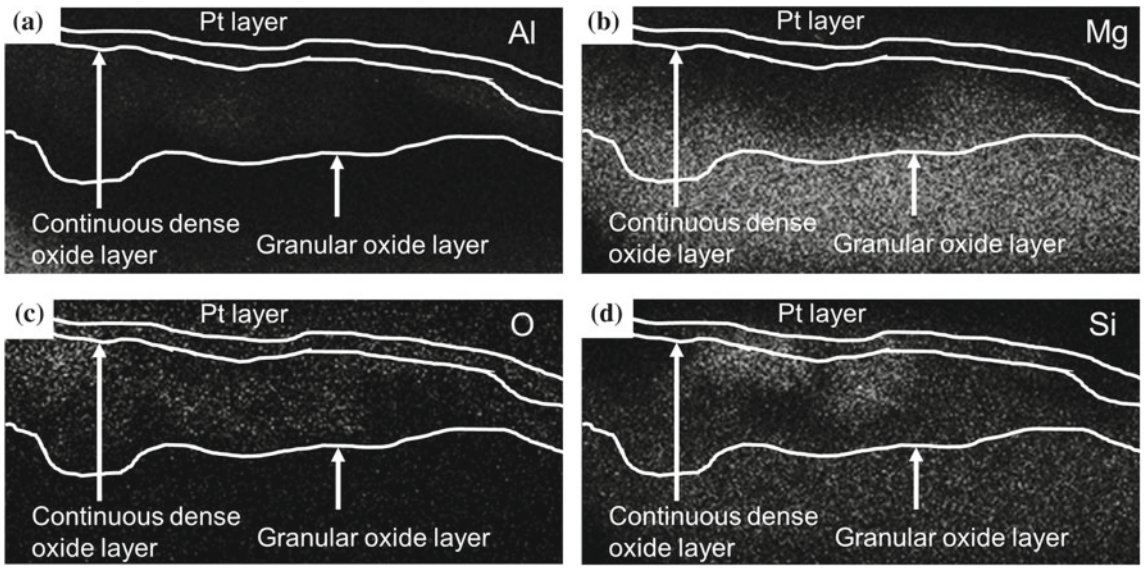

Fig. 5 EDS analysis of the AlMgSi discs heated at 750 °C for 7 h in 4% CO_2 of **a** Al, **b** Mg, **c** O and **d** Si, showing a dense oxide layer of Al, O and partly Si, and a Mg rich granular oxide layer with Al, O and Si

not as significant as the peaks obtained in the case of the discs heated in synthetic air and Ar. Through the microscopic evaluation the existence of a clear texture and cracks on the surface of the heated discs become visible at a magnification of 1000×, see Fig. 3c. The cross section seen in Fig. 4b reveals a two-layered oxide region consisting of a 200–400 nm thick continuous dense oxide layer with an additional ~2 µm granular oxide layer underneath. The region at which the EDS analysis was performed is marked with a dashed white rectangular in Fig. 4b, and the results reveal the presence of Al, Mg, O and Si in the oxide layer. The elemental mapping seen in Fig. 5a–d, confirms the presence of Al, O and Si in the upper region of the cross section, i.e. close to the continuous dense oxide layer, which may be due to formation of Al_2O_3 and Si (s). This occurs locally creating a high Si concentration, which allows precipitation of Si crystals during solidification as a consequence of low activity of Mg in the melt. An increase of Mg as a function of depth into the granular oxide layer is observed, and a region with higher concentration of Mg and Si is identified to exist. According to the phase diagram, Mg_2Si may be formed as a result of the lower activity of Al at the interface between the granular oxide layer and the bulk metal. This also correlates with the low heat flux detected after ~3 h (Fig. 2d), compared to the more negative peaks measured for synthetic air (Fig. 2b) and Ar (Fig. 2c) generating MgO, $MgAl_2O_4$ and Mg_2SiO_4, i.e. lower ΔG^0 values causing deeper heat flux peaks than for Mg_2Si. As a result, the 200–400 nm thin oxide layer formed on the surface of the heated AlMgSi discs is comparable with the findings of a similar layer established to exist for Al_5Mg when heated in a cover gas containing small amounts of CO_2, retarding the evaporation of Mg towards the surface and the overall formation of the oxide layer [2]. Further investigations are, however, needed to verify the results using Transmission Electron Microscope (TEM) and X-ray Photoelectron Spectroscopy (XPS).

Conclusion

An AlMgSi alloy has been investigated using a DSC-TG apparatus at 750 °C for 7 h in three different cover gases, i.e. (i) 20% pure Ar and 80% synthetic air, (ii) 99.999% pure Ar, and (iii) a gaseous mixture of 20% pure Ar, 76% synthetic air and 4% CO_2. The rate of oxidation has been monitored in regards of mass gain (TGA) and heat flux (DSC), and further evaluation have been carried out by microscopic analyses. A decrease in the mass gain from 12.33% to 2.80% was measured when changing the cover gas from synthetic air to pure Ar. The thickness of the oxide layer also decreased from >15 µm to ~10 µm, where the phases present in the oxide layers changed from MgO, $MgAl_2O_4$ and Mg_2SiO_4 to only MgO. A cover gas containing 4% CO_2 proved to have a significant inhibiting effect on the rate of oxidation, resulting in a mass gain of only 0.46%. In this case a continuous dense oxide layer with a thickness of 200-400 nm, covering an additional ~2 µm thick granular oxide layer, were identified to exist. The dense layer proved to consists of Al_2O_3 and Si (s), and the interface between the granular layer and the bulk of Mg_2Si and pure Si (s), which were the result of the low activity of Mg and Al, respectively.

Future Work

Future work will include investigations of the oxide layers formed during heat treatment of the AlMgSi discs during exposure to different cover gases, i.e. synthetic air, pure Ar and gaseous mixtures of Ar, synthetic air and CO_2. TEM and XPS will be used to confirm the mechanisms involved in the formation of the oxide layers by evaluating the chemical composition and morphology of the layers, as well as the overall behavior of Si. Experiments varying the relative concentrations of Mg and Si in the alloy will also be carried out to get a more comprehensive understanding of how the chemical composition and cover gas affect the oxidation rate. The holding time of the isothermal segment will be increased, to allow for the evaluation of any breakaway oxidation for the AlMg-, AlSi- and AlMgSi-based alloys.

Acknowledgements The authors would like to thank the Department of Materials Science and Engineering at the Norwegian University of Science and Technology (NTNU), Trondheim, Norway, the Centre for Research-Based Innovation (SFI Metal Production), and the Research Council of Norway (NFR Project number 237738) for funding the project.

References

1. K. Surla, F. Valdivieso, M. Pijolat, M. Soustelle, and M. Prin, "Kinetic study of the oxidation by oxygen of liquid Al–Mg 5% alloys," *Solid State Ionics*, vol. 143, no. 3, pp. 355–365, Jul. 2001.
2. N. Smith, B. Gleeson, W. A. Saidi, A. Kvithyld, and G. Tranell, "Mechanism behind the Inhibiting Effect of CO_2 on the Oxidation of Al–Mg Alloys," *Ind. Eng. Chem. Res.*, vol. 58, no. 3, pp. 1434–1442, Jan. 2019.
3. D. L. Belitskus, "Oxidation of molten Al-Mg alloy in air, air-SO_2, and air-H_2S atmospheres," *Oxid Met*, vol. 3, no. 4, pp. 313–317, Jul. 1971.
4. G. Wightman and D. J. Fray, "The dynamic oxidation of aluminum and its alloys," *MTB*, vol. 14, no. 4, pp. 625–631, Dec. 1983.
5. N. Ünlü and M. G. Drouet, "Comparison of salt-free aluminum dross treatment processes," *Resources, Conservation and Recycling*, vol. 36, no. 1, pp. 61–72, Jul. 2002.
6. N. Smith, "Methods of oxidation inhibition for Al–Mg alloys," Ph. D. Thesis, NTNU, Norwegian University of Science and Technology, Trondheim, 2019.
7. C. N. Cochran, D. L. Belitskus, and D. L. Kinosz, "Oxidation of aluminum-magnesium melts in air, oxygen, flue gas, and carbon dioxide," *MTB*, vol. 8, no. 1, pp. 323–332, Mar. 1977.
8. H. Venugopalan and T. DebRoy, "Kinetics of directed oxidation of Al-Mg alloys into $A1_2O_3$ preforms," *Materials Science and Engineering: A*, vol. 232, no. 1, pp. 39–46, Jul. 1997.
9. C. Blawert, N. Hort, and K. U. Kainer, "AUTOMOTIVE APPLICATIONS OF MAGNESIUM AND ITS ALLOYS," *TRANS. INDIAN INST. MET.*, vol. 57, no. 4, p. 12, 2004.
10. C. N. Cochran and W. C. Sleppy, "Oxidation of high-purity aluminum and 5052 aluminum-magnesium alloy at elevated temperatures," *J. Electrochem. Soc.*, vol. 108, no. 4, pp. 322–327, Apr. 1961.
11. I. Haginoya and T. Fukusako, "Oxidation of molten Al–Mg alloys," *Trans. JIM*, vol. 24, no. 9, pp. 613–619, 1983.
12. J. Steglich, C. Matthies, M. Rosefort, and B. Friedrich, "Behavior of Mg–Si-rich phases in aluminum can sheets and their impact on metal oxidation during industrial thermal pre-treatment," in *Light Metals 2018*, 2018, pp. 1123–1130.
13. N. Smith, A. Kvithyld, and G. Tranell, "The mechanism behind the oxidation protection of high Mg Al alloys with beryllium," *Metall and Materi Trans B*, vol. 49, no. 5, pp. 2846–2857, Oct. 2018.
14. *HSC Chemistry 9*. Outotec Technologies.
15. *FactSage Version 7.1*.